New Applications and Advances of the GPS Radio Occultation Technology as recovered by Analysis of the FORMOSAT-3 and CHAMP Data-Base

A.G. Pavelyev[1], Y.A. Liou[2], J. Wickert[3], V.N. Gubenko[1], A.A. Pavelyev[1], S.S. Matyugov[1]

[1] Institute of Radio Engineering and Electronics of the Russian Academy of Sciences, (IRE RAS), Fryazino, Vvedenskogo sq. 1, 141191 Moscow region, Russia
E-mail pvlv@ms.ire.rssi.ru Phone: +7-496-56-255-55; Fax: +7-495-702-75-92
[2] Center for Space and Remote Sensing Research, National Central University, Chung-Li, 320, Taiwan.
E-mail: yueian@csrsr.ncu.edu.tw Phone: +886 3 4227151 ext. 57631; Fax: +886 3 4254908
[3] GeoForschungsZentrum Potsdam (GFZ-Potsdam), Telegrafenberg, 14473 Potsdam Germany
E-mail: wickert@gfz-potsdam.de Phone: +49- 331-288-1168; Fax: +49-331-288-1169

Abstract Comparative analysis of the phase and amplitude variations of the GPS radio-holograms allows one to separate the influence of the layered and irregular structures. A possibility exists to measure important parameters of the internal waves: the intrinsic phase speed, the horizontal wind perturbations and, under some assumptions, the intrinsic frequency as functions of height in the atmosphere. A new technique was applied to measurements provided during CHAllenging Minisatellite Payload (CHAMP) and the Formosa Satellite-3 and Constellation Observing System for Meteorology, Ionosphere, and Climate (FORMOSAT-3/COSMIC) radio occultation (RO) missions. As an example of this approach, we establish the atmospheric origin of the amplitude and phase variations in RO signal at the altitudes 10 – 26 km. We observed for the first time in the RO practice examples of the internal wave breaking at the altitudes between 38 and 45 km. We obtained the geographical distributions and seasonal dependence of the atmospheric wave activity with global coverage for period 2001 – 2003 years.

1 Introduction

Atmospheric gravity waves (GW) have been a subject of intense research activities in recent years because of their various effects and their major contributions to atmospheric circulation, structure, and variability (Fritts and Alexander, 2003). Radiosonde and rocketsonde GWs measurements, balloon soundings, radar observations and lidar studies have been limited to ground-based sites (Fritts et al., 1988, Wilson et al., 1991, Eckermann et al., 1995, Steiner and Kirchengast, 2000, Tsuda et al., 2004, Wang et al., 2005) mainly over specific land parts of the Northern and Southern Hemispheres.

The radio occultation technology incorporates high-precision GPS radio signals at two frequencies (F1=1575.42 and F2=1227.6 MHz) for the investigation of internal waves. It allows the analysis of phase and amplitude of the radio waves after their propagating through the atmosphere. Analysis of the temperature variations found from the RO phase data furnishes an opportunity to measure the GW's statistical characteristics in the atmosphere (Steiner and Kirchengast, 2000, Tsuda et al., 2000, 2004, Tsuda and Hocke, 2002). Of particular importance are new ways to investigate locations of the layered plasma structures in the ionosphere. Radio holographic methods for the analysis of RO signals have the potential and capability for the research and simultaneous observation of the atmospheric and ionospheric waves (Igarashi et al., 2000, 2001, Pavelyev et al., 2002, 2003, 2004, Liou et al., 2002, 2003,2006). However up to now the assumption of the global spherical symmetry of the atmosphere and ionosphere is a cornerstone in the analysis of GPS RO measurements (Hajj et al., 2002, Wickert et al., 2004).

The aim of this paper is to introduce a new technique for estimating parameters of the internal waves, to demonstrate the examples of direct observation and location of the quasi-regular internal waves, and to analyze the seasonal and geographical distributions of the internal wave activity at different levels in the atmosphere using the amplitude and phase variations in the GPS occultation signals.

2 Radio occultation method

The scheme of the RO geometry is shown in Fig. 1. The point O is the center of the global spherical symmetry of the Earth's atmosphere and ionosphere. Radio waves emitted by the GPS satellite (point G) arrive at the receiver on board of the LEO satellite (point L) along the ray GTL, where T is the tangent point in the atmosphere. The results of registration which are the 1-D radio-holographic images of the propagation medium consist of the phase path excesses $\Phi_1(t)$ and $\Phi_2(t)$ along the amplitudes $A_1(t)$ and $A_2(t)$ of the radio field as functions of time at two GPS frequencies. These variations are caused mainly owing to the medium influence at the tangent point T, where the refractivity gradient is perpendicular to the ray GTL (Fig. 1). In the case of spherical symmetry the point T coincides with the perigee of ray GTL, where the distance from the center of spherical symmetry – point O is minimal and equal to r_0. The geographical coordinates of the ray perigee can be evaluated by use of orbital data of the GPS and LEO satellites. Analysis of RO data delivers the vertical profile of the refractivity $N(h)$ in the atmosphere and then the vertical profiles of pressure $p(h)$ and temperature $T(h)$.

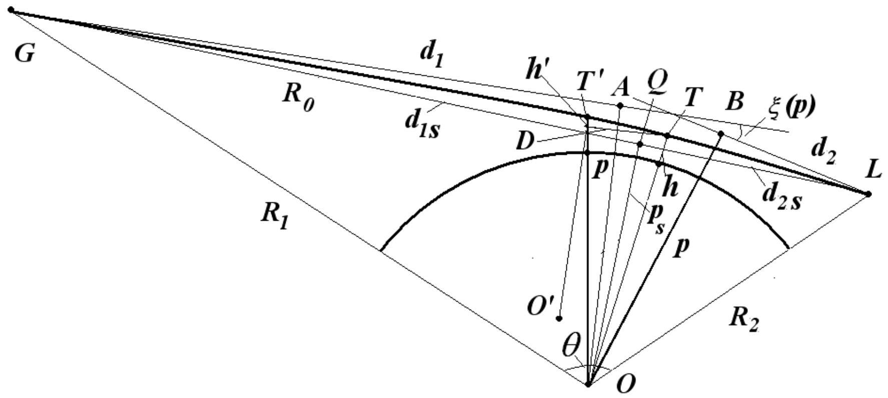

Fig. 1 Key geometrical parameters for RO measurements.

The projection of the point T on the Earth's surface determines the geographical coordinates of the RO region. The vertical velocity of the occultation beam path $v_\perp$ is about of 2 km/s. This value of $v_\perp$ is many times greater than those corresponding to the motion of layers in the ionosphere and atmosphere. Thus the RO radio-holograms record practically simultaneously the impact of the internal waves on the RO signal because the vertical displacement of a wave structure is negligible during the moving of the beam across it. However the horizontal gradients in the atmosphere and ionosphere can disturb the spherical symmetry of the atmosphere and ionosphere (Wickert et al., 2004). Actually a local spherical symmetry can exist for inclined layered structures in the propagation medium. In the case of the local spherical symmetry one can use the same relationships, which have been previously obtained for the case of the global spherical symmetry (Pavelyev et al., 2002, 2004) with a change of the designation of the impact parameter from p to p' (Fig. 1). For simplicity we will not use the primes on p and O below.

In the case of local spherical symmetry with center at point O (Fig. 1) there are fundamental relations between the phase path excess $\Phi(p)$ [m] and the refraction attenuation of radio waves $X(p)$ (dimensionless), which characterizes the decreasing/increasing of the intensity of radio waves because of the influence of the refraction effect in the atmosphere (Pavelyev et al., 2002, 2004, Liou et al., 2006)

$$\Phi(p) = L(p) + \kappa(p) - L_0, \quad L(p) = d_1 + d_2 + p\xi(p), \qquad (1)$$

$$X(t) = pR_0^2\left[R_1R_2d_1d_2\sin\theta\left|\frac{\partial\theta}{\partial p}\right|\right]^{-1} \quad (2)$$

$$\frac{\partial\theta}{\partial p} = \frac{d\xi}{dp} - \left(\frac{1}{d_1}+\frac{1}{d_2}\right) \quad (3)$$

$$\Phi(p) = \left(R_1^2-p^2\right)^{1/2} + \left(R_2^2-p^2\right)^{1/2} + p\xi(p) + \kappa(p) - R_0 \quad (4)$$

$$R_0 = d_1 + d_2,\ d_{1,2} = \left(R_{1,2}^2-p^2\right)^{1/2} \quad (5)$$

where $\kappa(p)$ is the main refractivity part of the phase path excess, $\xi(p)=-d\kappa(p)/dp$ is the refraction angle, $\theta(p)$ is the central angle, p, p_s are the impact parameter of the ray trajectory *GTL*, and the line of sight *GQL*, respectively, R_0, R_1, R_2 are the distances *GL*, *OG*, and *OL*, correspondingly, $L(p)$ is the distance *GABL*. $L(p)$ is a sum of two short lengths *GA* (d_1), *BL* (d_2), and arc *AB* which is equal to the product $p\xi(p)$. Because smallness of the refraction effect the distances d_1, d_2 are approximately equal to *GQ* and *QL* (Fig. 1). According to equation (1) the phase path excess $\Phi(p)$ contains only one term $\kappa(p)$ which depends directly on the refractivity. This justifies the designation "main refractivity part" for $\kappa(p)$. The refraction angle $\xi(p)$ is connected with the central angle θ (Fig. 1):

$$\theta = \pi + \xi(p) - \sin^{-1}\left(\frac{p}{R_1}\right) - \sin^{-1}\left(\frac{p}{R_2}\right), \quad (6)$$

$$\theta = \pi - \sin^{-1}\left(\frac{p_s}{R_1}\right) - \sin^{-1}\left(\frac{p_s}{R_2}\right), \quad (7)$$

$$\xi(p) = \sin^{-1}\left(\frac{p}{R_1}\right) + \sin^{-1}\left(\frac{p}{R_2}\right) - \sin^{-1}\left(\frac{p_s}{R_1}\right) - \sin^{-1}\left(\frac{p_s}{R_2}\right), \quad (8)$$

Two different expressions (6) and (7) can be used to obtain the connections between the impact parameters p_s and p and the refraction angle $\xi(p)$. From equations (1) and (6), (7) one can obtain by time differentiation of the phase excess $\Phi(p)$ and the central angle θ the relationship connecting the Doppler frequency F_d of the RO signal with the impact parameters p and p_s:

$$\frac{d\Phi}{dt} = \lambda F_d = p\frac{d\theta}{dt} + \frac{dR_1}{dt}\left(1-\frac{p^2}{R_1^2}\right)^{1/2} + \frac{dR_2}{dt}\left(1-\frac{p^2}{R_2^2}\right)^{1/2} - \frac{dR_0}{dt}, \quad (9)$$

$$\frac{dp_s}{dt} = \frac{d_{1s}d_{2s}}{R_0}\left[-\frac{d\theta}{dt} + \frac{p_s}{R_1d_{1s}}\frac{dR_1}{dt} + \frac{p_s}{R_2d_{2s}}\frac{dR_2}{dt}\right], \quad (10)$$

$$d_{1s} = \left(R_1^2-p_s^2\right)^{1/2},\ d_{2s} = \left(R_2^2-p_s^2\right)^{1/2}, \quad (11)$$

where d_{1s}, d_{2s} are the distances GQ and QL, correspondingly, (Fig. 1). After substitution of the equation (10) into equation (9) one can obtain:

$$F_d = (p-p_s)\left[\left(\frac{1}{d_{1s}}+\frac{1}{d_{2s}}\right)\frac{dp_s}{dt} + (p-p_s)^2 (Q_1 + Q_2)\right]$$
$$Q_{1,2} = R_{1,2}\frac{dR_{1,2}}{dt}\left[d_{1s}d_{2s}(d_{1s}+d_{2s})(p_s d_{1s} d_{2s})\right]^{-1} \quad (12)$$

Equations (9) – (12) are valid for general case of the non-circular orbits of the GPS and LEO satellites. Usually in RO experiments the absolute values of difference $p-p_s$ and vertical velocities $dR_{1,2}/dt$ are far below (by factor 10^{-2}-10^{-4}) the absolute magnitudes of the impact parameter p (or p_s) and vertical velocity of ray perigee dp_s/dt. Under condition $|(p-p_s)dR_{1,2}/dt| << p_s |dp_s/dt|$ one can obtain from equation (12) a simple formula for estimation of the difference $p-p_s$ on the Doppler frequency

$$F_d = (p-p_s)\left(\frac{1}{d_{1s}}+\frac{1}{d_{2s}}\right)\frac{dp_s}{dt}. \quad (13)$$

The values p_s, dp_s/dt, d_{1S}, d_{2S} can be delivered from the orbital data, and the phase delays $\Phi_{1,2}(p)$ are the objects of measurements and given in the phase parts of radio-holograms at frequencies F1 and F2. Below we will consider new relationships, which connect the phase acceleration $a=d^2\Phi(t)/dt^2$, Doppler frequency $F_d(t)$ and refraction attenuation of radio waves $X(t)$. Under conditions

$$|p-p_s| << p_s, \quad \left|\frac{(p-p_s)\,d\left(\frac{\partial\Phi}{\partial p_s}\right)}{dt}\right| << \left|\left(\frac{dp}{dt}-\frac{dp_s}{dt}\right)\frac{\partial\Phi}{\partial p}\right|, \quad (14)$$

by use of equation $dp/dt-dp_s/dt \approx [X(t)-1]dp_s/dt$ (*Liou et al.*, 2006), one can obtain from (13):

$$1-X(t) = m\frac{dF_d}{dt} = m\frac{d^2\Phi}{dt^2} = ma, \quad (15)$$

$$m = \left(\frac{dp_s}{dt}\right)^{-2}\frac{d_1 d_2}{(d_1+d_2)}, \quad (16)$$

Equations (15), (16) relate the refraction attenuation and the excess phase path acceleration via a classical dynamics equation-type and first published in 2006 (Liou and Pavelyev, 2006). The coefficient m, having dimension [s^2/m], is a slowly changing function of the vertical velocity dp_s/dt of the ray perigee T and distances d_1, d_2. Equation (15) indicates equivalence between the variations of the excess phase path acceleration a, derivative of the Doppler frequency $F_d(t)$, and refraction attenuation $X(t)$. Usually during the RO experiments parameters m and

dp_s/dt are known from the orbital data because the location of the spherical symmetry centre O and its projection on the line of sight – point Q are supposed to be known, and the distance GT d_1 and TL d_2 can be estimated as $d_{1,2}=(R_{1,2}^2-p^2)^{1/2}$ (Fig. 1). Therefore, equation (15) gives a possibility to recalculate the phase acceleration a and/or Doppler frequency F_d to the refraction attenuation X_p. This is useful for excluding the systematic errors from the phase and/or amplitude data. This is also useful for the estimation of the absorption in the atmosphere. The refraction attenuation X_a is determined from the amplitude data as a ratio of the intensity of radio waves propagating through the atmosphere $I_a(t)$ to its intensity in free space I_s:

$$X_a(t)=\frac{I_a(t)}{I_s} \tag{17}$$

The experimental value X_a (dimensionless) is the product of the refractive and absorption contributions. However, the phase acceleration depends on the refraction effect only. This gives a possibility to determine the absorption in the atmosphere $Y(t)$ as a ratio:

$$Y(t)=\frac{X_a(t)}{(1-m)a}, \quad X_p(t)=1-m\frac{da}{dt}. \tag{18}$$

This possibility must be investigated in detail because in future satellite RO missions the measurements of the absorption effects due to water vapor and minor atmospheric gas constituents are planning, and the difficulties will consist of removing the refraction attenuation effect from the amplitude data. Equations (18) indicate the feasible way to solve this problem. Also the relationships (18) may be useful for estimation the conditions for communication in the Ku/K bands between two LEO satellites in a radio occultation geometry (Martini et al., 2006).

The phase variations of the RO signal as function of time $\Phi(t)$ at each GPS frequency F1 and F2 contain slowly and quickly changing parts $\Phi_s(t)$ and $\Phi_f(t)$:

$$\Phi(t)=\Phi_s(t)+\Phi_f(t) \tag{19}$$

After substitution of formula (19) in equation (15) one can obtain:

$$1-X_p(t)=m\left[\frac{d^2\Phi_s(t)}{dt^2}+\frac{d^2\Phi_f(t)}{dt^2}\right]\approx m\frac{d^2\Phi_f(t)}{dt^2}, \tag{20}$$

Equation (20) is valid under condition: $|d^2\Phi_s(t)/dt^2|<<|d^2\Phi_f(t)/dt^2|$, which is fulfilled if the influence of the irregularities in the atmosphere and ionosphere is far below the effect of the standard atmosphere (or ionosphere) near the ray perigee. The contribution of layered structures to the phase excess variations in some cases may be considered as a quasi-periodical process, and the second derivative $d^2\Phi(t)/dt^2$ may be presented in the form:

$$\frac{d^2\Phi_f(t)}{dt^2}\approx-\omega^2\Phi_f(t), \quad \omega^2=4\pi^2F_v^2 \tag{21}$$

where v_p – is the vertical velocity of the RO ray near the perigee T (Fig.1). Parameter $\omega_0^{\,2}$ depends on the vertical period λ_v of layered structure. After substitution of expression (21) in equation (15) one can obtain:

$$X(t) - 1 = c_0 \Phi_f(t),\ c_0 = m\omega_0^{\,2} = k_v^{\,2} d_1 d_2/R_0,\ k_v^{\,2} = 4\pi^2/\lambda_v^2, \qquad (22)$$

where k_v is the vertical wave number of the vertical quasi-periodical structure in the ionosphere (atmosphere), d_1, d_2 are the distances along the ray GTL from the point L and G up to the ray perigee T, respectively, R_0 is the distance GL (Fig. 1). Equation (22) connects the high-frequency part of the phase path excess variations $\Phi_f(t)$ with the refraction attenuation changes $X(t)-1$ of the RO signal. Note, that the coefficient c_0 in equations (22) does not depend on the vertical velocity of the ray perigee. Equation (22) allows one to recalculate the refraction attenuation variations of the GPS radio-holograms to the phase path excess variations and vice versa. The form of the phase path excess variations $\Phi_f(t)$ is similar to the form of the intensity variations $X(t)-1$. It follows from equations (22) that variations of the intensity of RO signal are proportional to the phase path excess oscillations and inversely proportional to the second power of the vertical spatial period of layered structure. One can estimate from equations (22) the value of parameter c_0 by comparison of the amplitude and phase variations of RO signal.

As follows from our analysis the practical algorithm for revealing the contribution of the lower ionosphere in the phase data can be described by equation:

$$\Phi_l(t) = \Phi(t) - \langle \Phi(t) \rangle, \qquad (23)$$

where $\langle \Phi(t) \rangle$ denotes the trend in the phase data. Alternative approach to find $\langle \Phi(t) \rangle$ consists in averaging of the phase path excess over a sliding interval, the size of the sliding averaging interval must be long enough to account for the long-scale influence of the atmosphere or upper ionosphere.

Usually during RO experiments parameter m (eqs. (15), (16)) is a slowly changing function of time. Parameter dp_s/dt depends on the velocity components v, w of the GPS and LEO satellites, respectively. Components v, w are perpendicular to the straight line GL in the plane GOL. The components v, w are positive when oriented in direction to the point O and are negative in the opposite case. Components v, w are connected with parameter dp_s/dt by equation:

$$d\,p_S/dt = v + (w - v)\, d_{1S}/R_0, \qquad (24)$$

Equations (15), (16) and (24) can be used to find the distance LT d_{2s} from simultaneous observations of the phase and intensity variations of radio waves. To achieve this, one can find m from (15) from the ratio of the refraction attenuation changes to the phase acceleration variations and then the distance d_{2S} can be evaluated from the relationship:

$$d_{2S} = 2mw^2\,[1 + 2b\,(v/w - 1) + (1 - 4b\, v/w)^{1/2}]^{-1},\ b = mw^2/R_0, \qquad (25)$$

Relations (15), (25) may be applied for the location of the tangent point T (or locally spherical symmetric layers) in the propagation medium.

3 Connection between the phase acceleration and intensity variations: experimental validation

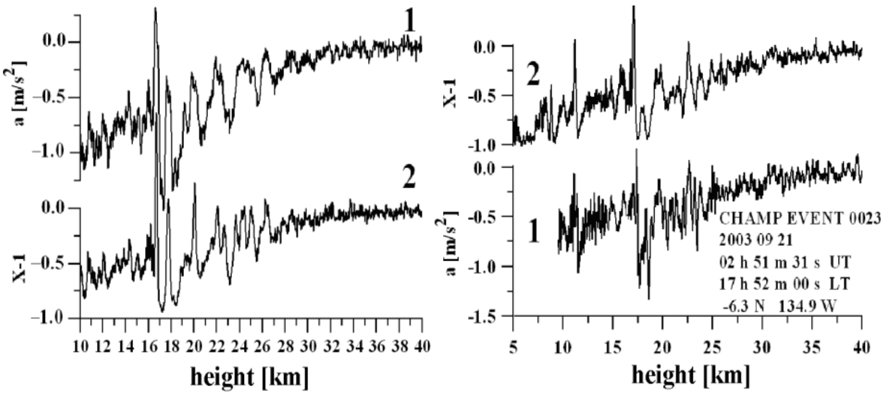

Fig. 2 Phase acceleration a and refraction attenuation variations $X–1$ at the first GPS frequency F1 (curves 1 and 2, respectively) for two CHAMP RO events: № 0136 on January 14, 2003 (left panel) and № 0023 on September 21, 2003 (right panel).

The phase acceleration a calculated as the second temporal derivative of the phase path excess and intensity variations $X(t)–1$ at the frequency f_1 are shown in Fig. 2 (curves 1 and 2, respectively) for the CHAMP RO events 0136 (January 14, 2003) and 0023 (September 21, 2003). As seen in Fig. 2, there is a good correspondence between variations of the phase acceleration and the refraction attenuation of the RO signal. The coefficient m is different in the RO events 0136 and 0023. The average ratio of the refraction attenuation and the phase acceleration m is about 1.0 [s^2/m] in the 5 – 40 km height interval for the RO event 0136 (Fig. 2, left panel) but for event 0023 (Fig. 2, right panel) is about 1.5 times greater. As follows from orbital data, the change in parameter m during these RO events is about 10%. As follows from analysis of data shown in Fig. 2 the relationships (15), (16) are valid and they may allow one to locate the layered structures in the atmosphere and ionosphere, which are responsible for the variations of the intensity and phase acceleration of radio waves in the satellite-to-satellite links. An example of determination of the displacement $D= d_{2S}– d_2$ is shown in Fig. 3 for the FORMOSAT-3/COSMIC RO event 0006, April 23, 2006, 15 h 54 m 28 s LT, with geographical coordinates 9.5 S, 288.9 W. Curve 1 and 2 in Fig. 3, left panel, demonstrate good correspondence between the refraction attenuation X_p estimated from the phase acceleration a and parameter m by use of formula $1\text{-}X_p\text{=}ma$, and X_a evaluated from the amplitude data, respectively, at the first GPS frequency F1.

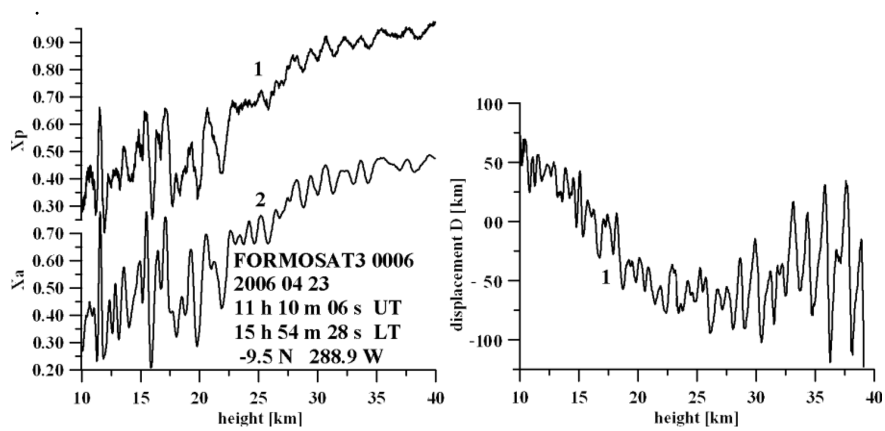

Fig. 3 Left panel. Comparison of the refraction attenuations X_a and X_p calculated from the phase (curve 1) and amplitude (curve 2) data. Right panel. Displacement D of the tangent point T calculated by use of equations (15), (25).

The results of evaluation of the displacement *D* by use of equations (15) and (25) are shown in Fig. 3, right panel (curve 1). According to Fig. 3 (right panel) the displacement *D* is bound between ±50 km in the 10 km – 25 km altitude interval and between ±100 km in the 25 km – 40 km height interval. It follows that the phase acceleration has the same importance for the RO experiments as the well-known Doppler frequency.

4 Wave- breaking effect and determination of internal wave parameters

The amplitude channel of the radio hologram can be used to obtain information on the vertical distribution of the refractivity, temperature, and its vertical gradient (Pavelyev et al., 2002, 2003, Liou et al., 2002, 2003, 2006). The amplitude variations of RO signal depend mainly on the high-frequency part of the derivative of the refraction angle on the impact parameter $d\xi(p)/dp$. For obtaining the corresponding variations in the vertical gradient of refractivity $dN(h)/dh$ the low frequency part in the function $d\xi(p)/dp$ corresponding to the low frequency noise in the amplitude data have been excluded by numerical filtration. The remaining high-frequency part of $d\xi_h(p)/dp$ was transformed by use of the Abel' transformation technique (Liou et al., 2002), to find perturbations in the vertical gradient of refractivity $dN_h(h)/dh$. This procedure is not needed an optimization technique because (1) absence of the low frequency noise in the function $d\xi_h(p)/dp$ and (2) high sensitivity of the amplitude to the high-frequency variations in the vertical gradient of refractivity (variations of the intensity of RO signal are inversely proportional to the second power of the vertical spatial period of layered structure).

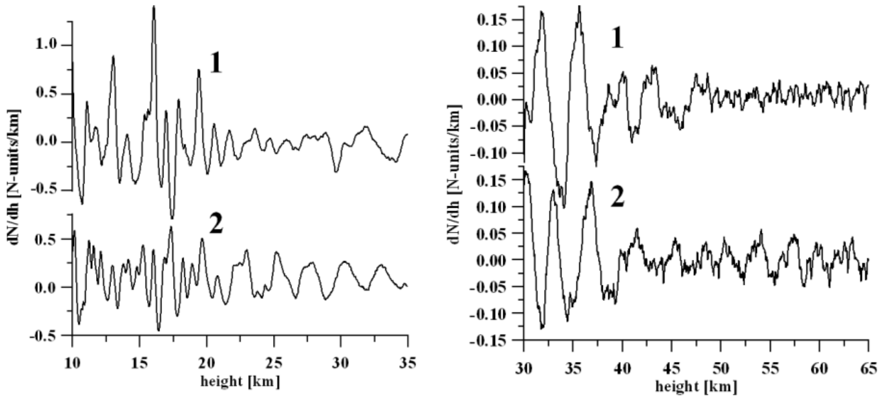

Fig. 4 Vertical gradient of refractivity perturbations at the first GPS frequency F1 in the 10 – 30 km (left) and 30 – 65 km height interval (right). Abrupt changes in the amplitude and phase of the refractivity perturbations are seen between the altitudes 38 and 40 km (curves 1 and 2, right panel) and 45 – 50 km (curve 1, right panel). Curves 1 and 2 correspond to CHAMP RO events № 0140 (02 h 35 m 34 s LT, 21.9 N 172.5 W) and № 0001 (02 h 09 m 51 s LT, 15.9 N 330.0 W), January 23, 2003, respectively.

Variations in the vertical gradient of refractivity retrieved from the RO amplitude data are shown in Fig. 4 for CHAMP RO events № 0140 and № 0001, January 23, 2003 (curves 1 and 2, respectively). The wave structure is clearly seen in the perturbations of the vertical refractivity gradient in the 10 – 45 km interval (curve 1 and 2, left and right panels in Fig. 4). The vertical period of the wave structure grew from 0.8-1.0 km in the 10-25 km interval to 2-4 km in the 30-40 km interval. Abrupt changes in the amplitude and phase of the refractivity perturbations are seen between the altitudes 38 and 40 km (curves 1 and 2, right panel) and 45 – 50 km (curve 1, right panel). These changes may be connected with wave-breaking altitudes where the wave energy dissipate to eddies and turbulence. Previously the wave breaking effect has been observed from space during CRISTA experiments (Eckermann and Preusse, 1999) at altitudes between 30 and 40 km. There are indications for GW breaking at altitudes of about 50–60 km (Ern et al., 2006). Note that phenomena of wave breaking shown in Fig. 4 are the first direct observations by use of the GPS RO method.

5. Integral behavior of wave activity in the years 2001-2003

The wave activity in the atmosphere over a global scale can be characterized by the RO index β: probability of strong wave amplitudes exceeding the fixed level of the vertical gradient of refractivity q. This index has a global importance for the description of wave activity in the atmosphere as seen in Fig. 5 and Fig. 6 based on the analysis of CHAMP RO data for the time period 2001 – 2003. The magni

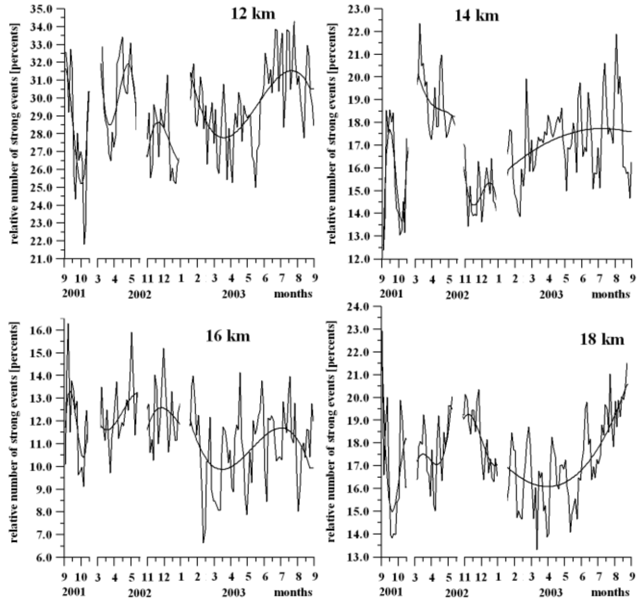

Fig. 5 Changes in internal waves activity (averaged over the Earth globe) during 2001 – 2003 years at different altitudes in the atmosphere: 12 km and 14 km (top left and right panels, respectively), 16 and 18 km (bottom left and right panels, respectively).

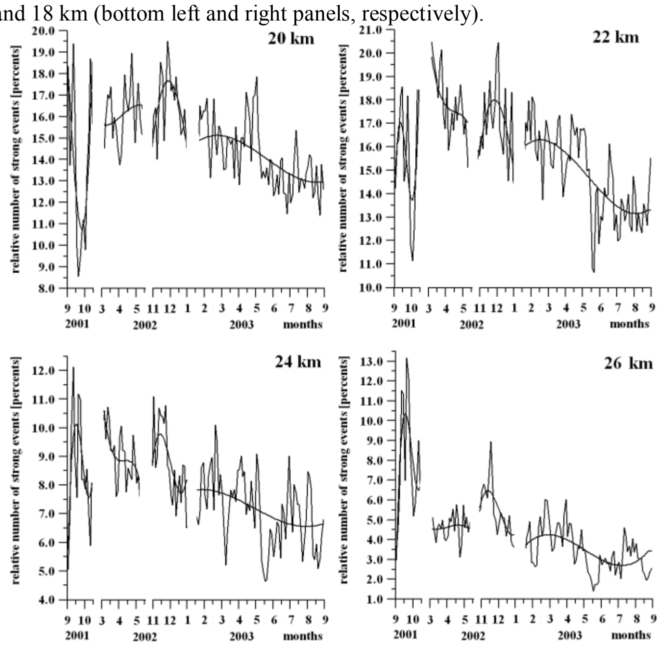

Fig. 6 Changes in internal waves activity (averaged over the Earth globe) during 2001 – 2003 years at different altitudes in the atmosphere: 20 km and 22 km (top left and right panels, respectively), 24 and 26 km (bottom left and right panels, respectively).

*t*ude β has been defined in this analysis as a ratio of numbers of intense wave amplitude greater than *q>0.6 N-units/km* for the 12 – 16 km and with *q>0.24 N-units/km* for the 18 – 26 km to total number of measurements over the Earth globe. The value β is marked in percents at vertical axis in Fig. 5 and Fig. 6. The smooth curves in Fig. 5 and Fig. 6 are obtained as approximation of the experimental data (broken lines in Fig. 5 and Fig. 6) by least squares method. The data, shown in Fig. 5 and Fig. 6, are relevant to three year time interval September 2001 – September 2003, with three data gaps: (1) from October 15, 2001, up to February 28, 2002; (2) from May 16, 2002, up to October 31, 2002; (3) from January 01 up to January 12, 2003. The seasonal and annual changes of wave activity are seen at all altitudes 12 – 26 km in Fig. 5 and Fig. 6. For example, changes with period of about 12 months are seen at the altitudes 12 km, 16 km, and 20 – 26 km (Fig. 5 and Fig. 6) for period January – September 2003. The phases of one-year oscillations at altitudes 12 and 16 km are opposite to the phases of wave activity variations at the heights 20 – 26 km (Fig. 5 and Fig. 6). The wave activity behavior at the altitudes 14 and 18 km is different from that at the heights 12 km, 16 km and 20 – 26 km. The wave activity at the height 14 and 18 km is increasing when the time goes to the end of the considered period – September 2003. This may be connected with the tropopause effects. Changes in the tropopause height, significant variations in the refractivity gradients near the tropopause, and other phenomena can produce strong scintillations in the amplitude variations of RO signal. Analysis of these effects is a task of future investigation. At the altitudes 12 km, 16 km, and 20 – 26 km the wave activity is gradually diminishing by 10% – 40% when the time changes from September 2001 to September 2003. This diminishing may be connected with changes in the intensity of the meteorological processes, types of the atmospheric circulations, and, very likely, with reduction in solar activity in the considered period of time. In that respect the internal waves activity may be considered among the other important parameters described in various publications (e.g. Suh and Lim, 2006, and references therein), which characterize effects of solar activity on the Earth atmosphere.

Conclusion

Comparative theoretical and experimental analysis of the phase and amplitude variations of the GPS radio-holograms discovered new relationships, which relate the refraction attenuation and the excess phase path acceleration via a classical dynamics equation-type. The advantages of the introduced relationship consist in (1) a possibility to separate the layered structure and turbulence contributions to RO signal; (2) a possibility to estimate the absorption in the atmosphere by dividing the refraction attenuations found from amplitude and phase data; (3) a possibility to locate the tangent point in the atmosphere with accuracy in the distance from the standard position of about ±100 km. The suggested method has a general importance (for example, it may be applied for analysis of the amplitude and phase variations in the trans-ionospheric satellite-to-Earth links). We showed also that the amplitude variations of GPS occultation signals are very sensitive sensors to the internal waves in the atmosphere. The sensitivity of the amplitude method is inversely proportional to the square of the vertical period of the internal wave, indicating high sensitivity of the amplitude data to the wave structures with small vertical periods in the 0.8-4 km interval. By use of the amplitude data analysis the internal wave breaking phenomenon has been observed at the first time in RO practice between 38 and 45 km altitudes.

The amplitude GPS occultation method presents a possibility to obtain the geographical distribution and seasonal dependence of the atmospheric wave activity with global coverage. At the altitudes 12 km, 16 km, and 20 – 26 km the wave activity is gradually diminishing by 10% – 40% from September 2001 to September 2003. This diminishing may be connected with changes in the intensity of the meteorological processes, types of the atmospheric circulations, and, very likely, with reduction in solar activity.

Acknowledgments We are grateful to the GeoForschungZentrum Potsdam for delivering the CHAMP RO data. We are grateful to the National Science Council of Taiwan, R.O.C., for financial support under the grants NSC 92-2811-M008-001, NSC 91-2111-M008-029, and the Office of Naval Research (ONR) of USA under grant N00014-00-0528. Work has been partly supported by the Russian Fund of Basic Research, grant No. 06-02-17071. In addition, assistance was provided by the Russian Academy of Sciences, program OFN-16 and OFN-17.

References

Eckermann SD, Hirota I, Hocking WA (1995) Gravity wave and equatorial wave morphology of the stratosphere derived from long-term rocket soundings. Q J R Meteorol Soc 121:149–186

Eckermann SD, Preusse P (1999) Global measurements of the stratospheric mountain waves from space. Science 286:1534–1537

Ern M, Preusse P, Warner CD (2006) Some experimental constraints for spectral parameters used in the Warner and McIntyre gravity wave parameterization scheme Atmos. Chem. Phys., 6: 4361–4381

Fritts DC, Tsuda T, Sato T, Fukao S, Kato S (1998) Observational evidence of a saturated gravity wave spectrum in the troposphere and lower stratosphere (1988) J. Atmos. Sci., 45: 1741–1759

Fritts DC, Alexander MJ (2003) Gravity wave dynamics and effects in the middle atmosphere. Rev Geophys 41:1–64

Hajj GA, Kursinski ER, Romans LJ, Bertiger WI, Leroy SS (2002) Technical description of atmospheric sounding by GPS occultation. J Atmos Solar-Terr Phys 64:451−469

Igarashi K, Pavelyev A, Hocke K, Pavelyev D, Kucherjavenkov IA, Matugov S, Zakharov A, Yakovlev O (2000) Radio holographic principle for observing natural processes in the atmosphere and retrieving meteorological parameters from RO data. Earth Planets Space 52: 968−875

Igarashi K, Pavelyev A, Hocke K, Pavelyev D, Wickert J (2001) Observation of wave structures in the upper atmosphere by means of radio holographic analysis of the RO data. Advances in Space Research 27(6-7): 1321−1327

Liou YA, Pavelyev AG (2006) Simultaneous observations of radio wave phase and intensity variations for locating the plasma layers in the ionosphere Geoph Res Lett 33(23), L23102, doi:10.1029/2006GL027112

Liou Y-A, Pavelyev AG, Huang C-Y, Igarashi K, Hocke K (2002) Simultaneous observation of the vertical gradients of refractivity in the atmosphere and electron density in the lower ionosphere by radio occultation amplitude method. Geophys Res Lett 29(19):1–43

Liou Y-A, Pavelyev AG, Huang C-Y, Igarashi K, Hocke K, Yan SK (2003), Analytic method for observation of the gravity waves using radio occultation data. Geophys Res Lett 30(20):1–5

Liou Y-A, Pavelyev AG, Wickert J, Liu SF, Pavelyev AA, Schmidt T, Igarashi K (2006) Application of GPS radio occultation method for observation of the internal waves in the atmosphere. J Geophys Res-Atmospheres 111(D06104):1−14

Martini E, Freni A, Facheris L, Cuccoli F 2006 Impact of tropospheric scintillation in the Ku/K bands on the communications between two LEO satellites in a radio occultation geometry. IEEE Trans Geosci Remote Sens 44(8): 2063−2071

Pavelyev AG, Liou YA, Wickert J (2004) Diffractive vector and scalar integrals for bistatic radio holographic remote sensing. Radio Sci 39(4):1−16, RS4011, doi:10.1029/2003RS002935

Pavelyev A, Igarashi K, Reigber C, Hocke K, Wickert J, Beyerle G, Matyugov S, Kucherjavenkov A, Pavelyev D, Yakovlev O (2002) First application of radioholographic method to wave observations in the upper atmosphere. Radio Sci 37(3):1–15

Pavelyev AG, Tsuda T, Igarashi K, Liou YA, Hocke K (2003) Wave structures in the electron density profile in the ionospheric D and E-layers observed by radio holography analysis of the GPS/MET radio occultation data. J Atmos Solar-Terr Phys 65(1):59−70

Suh Y-C, Lim G-H (2006) Effects of the 11-year solar cycle on the Earth atmosphere revealed in ECMWF reanalysis. Geophys Res Lett 33(24), L24705, doi:10.1029/2006GL028128.

Steiner A K, Kirchengast G (2000) Gravity wave spectra from GPS/MET occultation observations. J Atmos Ocean Tech 17:495–503

Tsuda T, Hocke K (2002) Vertical wave number spectrum of temperature fluctuations in the stratosphere using GPS occultation data. J Meteorol Soc Japan 80(4B):925–938

Tsuda T, Nishida M, Rocken C Ware RH (2000) A global morphology of gravity wave activity in the stratosphere revealed by the GPS occultation data (GPS/MET). J Geophys Res 105:7257–7273

Tsuda T, Ratnam MV, May PT, Alexander MJ, Vincent RA, MacKinnon A (2004) Characteristics of gravity waves with short vertical wavelengths observed with radiosonde and GPS occultation during DAWEX (Darwin Area Wave Experiment). J Geophys Res 109, D20S03, doi:10.1029/2004JD004946

Wang L, Geller MA, Alexander M J (2005) Spatial and temporal variations of gravity wave parameters. Part I: Intrinsic frequency, wavelength, and vertical propagation direction. J Atmos Sci 62:125–142

Wickert J, Pavelyev A G, Liou YA, Schmidt T, Reigber Ch, Igarashi K, Pavelyev AA, Matyugov SS (2004) Amplitude scintillations in GPS signals as a possible indicator of ionospheric structures Geophys Res Lett 31(24):1-4, L24801 doi:10.1029/2004GL020607

Wilson R, Chanin ML, Hauchecorne A (1991) Gravity waves in the middle atmosphere observed by Rayleigh lidar, 2. Climatology J Geophys Res 96, 5169-5183.